Quantum Electronics **48** (2) 184–187 (2018)

FIBRE-OPTIC SENSORS

https://doi.org/10.1070/QEL16541

Simultaneous optical fibre strain and temperature measurements in a hybrid distributed sensor based on Rayleigh and Raman scattering

B.G. Gorshkov, M.A. Taranov

Abstract. **A new type of sensor for simultaneous measurements of strain and temperature changes in an optical fibre is proposed. Its operation builds on the use of Raman optical time-domain reflectometry and wavelength-tunable quasi-monochromatic Rayleigh reflectometry implemented using a microelectromechanical filter (MEMS). The sensor configuration includes independent Raman and Rayleigh scattering channels. Our experiments have demonstrated that, at a sensing fibre length near 8 km, spatial resolution of 1–2 m, and measurement time of 10 min, the noise level (standard deviation) is 1.1 με (μm m^{-1}) for the measured tension change (at small temperature deviations) and 0.04 °C for the measured temperature change, which allows for effective sensing of mechanical and temperature influences with improved accuracy.**

Keywords: *distributed sensor, fibre-optic sensor, strain measurement, temperature measurement, reflectometry, wavelength tuning, Rayleigh scattering spectra, Raman scattering.*

1. Introduction

Fibre-optic distributed sensing systems have great potential for use in pipeline inspection and in monitoring the state of infrastructure facilities (bridges, dams and others). One topical issue is the ability to measure the mechanical strain and temperature in a system of interest. Moreover, a practical issue of vital importance is the ability to separately assess the effects of strain and temperature. Such a problem can in principle be resolved using Brillouin scattering, where the frequency shift and intensity of spontaneous Brillouin scattering lines are measured simultaneously [1]. Other approaches were also proposed [2, 3], but in most cases such systems have insufficient sensitivity. In this context, a number of studies focused on hybrid schemes, e.g. on those combining Brillouin and Raman scattering measurements [4, 5]. Using a 25-km length of optical fibre, Bolognini et al. [5] obtained a temperature resolution of 1.2 °C and strain resolution of 10^{-4} (100 με, or 100 μm m^{-1}), which approaches practical requirements, but is insufficient e.g. for civil infrastructure health monitoring [6].

Studies aimed at achieving higher sensitivity led to the advent of wavelength-tunable quasi-monochromatic Rayleigh reflectometry schemes. The idea of using such a scheme for strain measurements was first formulated by Froggatt and Moore [7]. Using a tunable-wavelength coherent optical time domain reflectometry (TW-COTDR) scheme, Koyamada et al. [8] demonstrated a 0.01 °C resolution, equivalent to a strain resolution of about 0.1 με (without separately assessing the contributions), with a 1-m spatial resolution. However, the cost of reaching such a result was a narrow dynamic range, 4 με, or 0.44 °C, in combination with a rather long (3 h) signal acquisition time. A solution proposed by us previously [9] allowed us to detect influences of up to 2000 με or 220 °C with an rms error of 2 με (0.22 °C) at a total measurement time of 10 min using a 8-km length of fibre, which is suitable for monitoring industrial facilities [6]. Nevertheless, the above-mentioned schemes [7–9] are incapable of separately assessing mechanical and temperature effects.

The purpose of this work is to study a new hybrid scheme for simultaneous strain and temperature sensing. The scheme allows one to simultaneously measure Rayleigh scattering spectra (like in a previous study [9]) and the power of spontaneous Raman scattering, which usually underlies distributed temperature measurements. Important advantages of the scheme are its high sensitivity and the possibility of utilising it when only one fibre end is accessible.

2. Operating principle of the sensor and the experimental setup

The operating principle of the proposed sensor builds on two physical effects. One of them is that tension/compression and heating/cooling of an optical fibre lead to a shift of its so-called Rayleigh scattering spectra. The term 'Rayleigh scattering spectrum' is here taken to mean the backscattered power spectrum of a given portion of the optical fibre, as obtained by scanning the input light frequency. The reflection spectrum of a Bragg grating can be defined in a similar manner. Figure 1 shows typical Rayleigh scattering spectra of a 1-m length of fibre, with a tension-induced shift relative to each other. The shift of the spectrum relative to its original position is proportional to the external stimulus: change in tension or temperature. Figure 2 shows the reduced normalised cross-correlation function of the original and shifted spectra displayed in Fig. 1. The shift of the centroid of its main peak with respect to the origin, $\Delta\lambda$, is numerically equal to the shift of the spectra. Thus, the problem of measuring the shift of the spectra algorithmically reduces to finding the position of the centroid of their cross-correlation function. This approach was described in detail elsewhere [9].

The other effect underlying the operating principle of the proposed sensor is spontaneous Raman scattering, in which

B.G. Gorshkov A.M. Prokhorov General Physics Institute, Russian Academy of Sciences, ul. Vavilova 38, 119991 Moscow, Russia; e-mail: bggorshkov@gmail.com;
M.A. Taranov PetroFibre Ltd, Klinskii proezd 7, 301664 Novomoskovsk, Tula region, Russia; e-mail: tarma@petrofibre.ru

Received 19 October 2017; revision received 28 November 2017
Kvantovaya Elektronika **48** (2) 184–187 (2018)
Translated by O.M. Tsarev

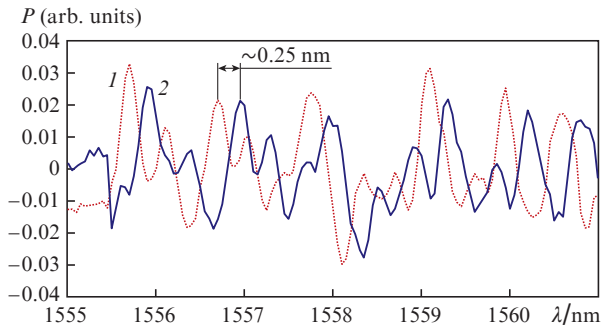

Figure 1. Rayleigh scattering spectra (with no constant component) measured at a bandwidth of 0.17 nm and a tuning step of 0.05 nm: (*1*) initial conditions, (*2*) tension of 200 με. The shift of the spectra is ~0.25 nm.

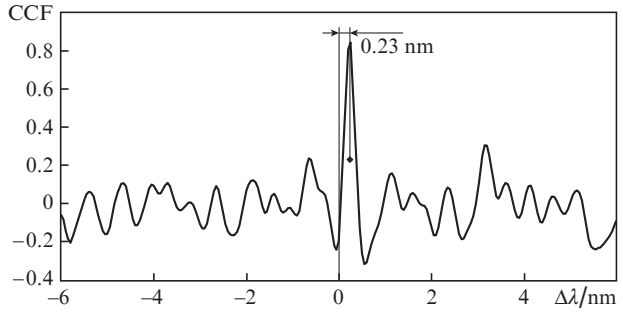

Figure 2. Reduced normalised cross-correlation function (CCF) of the spectra displayed in Fig. 1. The graph shows the shift $\Delta\Lambda$ of the centroid of the main peak of the function with a more accurate estimate of it.

the power of the Stokes and anti-Stokes signals depends significantly on the temperature of the fibre and is a weak function of its strain [10]. Since the temperature sensitivity of the anti-Stokes signal is about five times that of the Stokes signal [10], we recorded the former. Its power P_{RAS} as a function of absolute temperature T is known to have the form of the Bose–Einstein distribution and to be represented by the following mathematical expression:

$$P_{\mathrm{RAS}}(T) \propto \frac{\exp[-h\Delta\nu_{\mathrm{R}}/(k_{\mathrm{B}}T)]}{1-\exp[-h\Delta\nu_{\mathrm{R}}/(k_{\mathrm{B}}T)]}, \tag{1}$$

where h is the Planck constant; $\Delta\nu_{\mathrm{R}}$ is the frequency shift (about 13 THz for silica fibre); and k_{B} is the Stefan–Boltzmann constant. Instead of (1), we can use its linear least-squares fit, which has an error of at most 0.07 °C in the temperature range 25–45 °C, where our measurements were performed.

The above indicates that, simultaneously measuring the shift of Rayleigh scattering spectra, $\Delta\Lambda$, and the change in the anti-Stokes power normalised to that under the initial conditions, $\Delta P^{\mathrm{N}}_{\mathrm{RAS}}$, and solving a matrix equation of the form

$$\begin{bmatrix}\Delta\Lambda\\ \Delta P^{\mathrm{N}}_{\mathrm{RAS}}\end{bmatrix} = \begin{bmatrix}S^{\Lambda}_{\varepsilon} & S^{\Lambda}_{T}\\ S^{\mathrm{RAS}}_{\varepsilon} & S^{\mathrm{RAS}}_{T}\end{bmatrix}\begin{bmatrix}\Delta\varepsilon\\ \Delta T\end{bmatrix} \tag{2}$$

for changes in strain $\Delta\varepsilon$ and temperature ΔT, we will find the sought external influences on the fibre. This algorithm was implemented in the proposed sensor. In the matrix equation (2), $S^{\Lambda}_{\varepsilon}$ and S^{Λ}_{T} are respectively the strain and temperature sensitivities of the shift of the Rayleigh scattering spectra, and $S^{\mathrm{RAS}}_{\varepsilon}$ and S^{RAS}_{T} are respectively the strain and temperature sensitivities of the normalised anti-Stokes Raman signal.

Figure 3 shows a schematic of the experimental setup. As a pulsed light source, we used a Superlum SLD-761 superluminescent diode. The full width at half maximum (FWHM) of its emission spectrum was about 45 nm and its peak emission wavelength was approximately 1560 nm. The pulse duration was 10.5 ns, which ensured a spatial resolution near 1 m with no allowance for dispersion in the fibre. The pulse repetition rate was determined by the length of the test fibre (8 km) and was 12 kHz. The SLD power was amplified by an erbium-doped fibre amplifier (A1). To eliminate the sensor response instability resulting from the birefringence in the sensing fibre (SF), the system included a General Photonics PSM-002 polarisation scrambler (PS).

The key components of the scheme are thin-film wavelength-division multiplexers (WDM1 and WDM2) of the same type, which are used as directional spectral filters for separating the Rayleigh and Raman scattering channels (channels 1 and 2, respectively). The upper arm, formed by

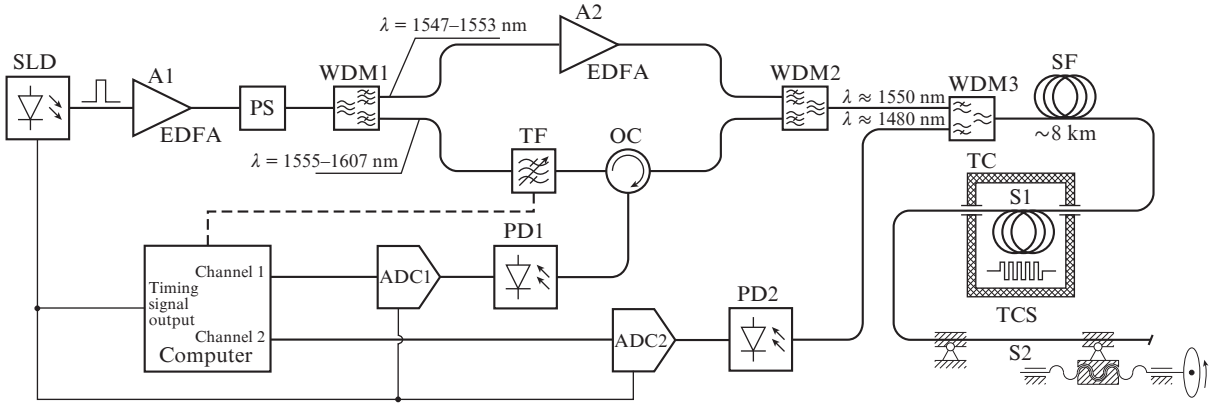

Figure 3. Schematic of the distributed strain–temperature sensor: (SLD) superluminescent diode; (A1, A2) amplifiers; (PS) polarisation scrambler; (WDM1–WDM3) wavelength-division multiplexers; (TF) tunable filter; (OC) optical circulator; (ADC1, ADC2) analog-to-digital converters; (PD1, PD2) photodetectors; (SF) sensing fibre; (TC) thermal chamber; (S1, S2) fibre segments; (TCS) tension control system.

the corresponding ports of the two multiplexers and having a transmission window from 1547 to 1553 nm, is used to deliver input light to the Raman scattering channel. The erbium-doped fibre amplifier A2, placed in this arm, is used to compensate for the loss of the power filtered off by WDM1 to the lower arm, which is formed by the ports with the transmission range 1555–1607 nm and includes the Rayleigh scattering channel. The choice of the ports with this transmission range for the Rayleigh channel is dictated by the fact that, after A1, the spectrum has a peak emission wavelength of 1558 nm, which falls in the range 1555–1607 nm. The channel includes a tunable spectral filter (TF), polarisation-insensitive optical circulator (OC) and photodetector (PD1). The TF is a DiCon MTF500B module based on a microelectromechanical system (MEMS), which controls the relative position of the mirrors, and a diffraction grating. The total tuning range of the filter is 1529–1564 nm and the full width at half maximum of its transmission band is 0.17 nm. PD1, which comprises a photodetector and transimpedance amplifier (TIA), has a 50-MHz transmission band.

The tunable filtration parameters – tuning range and step – determine, in large measure, the accuracy and speed of the sensor. Since the peak power wavelength in the emission spectrum at the TF input is 1558 nm, the tuning range was chosen to be 1558 ± 3 nm. Using data reported by Koyamada et al. [8], it can be estimated that tuning in the range ±3 nm corresponds to the strain and temperature ranges ±2500 με and ±275 °C, respectively. However, the fact that Rayleigh scattering spectra are measured in a finite range leads to a reduction in the amplitude of their cross-correlation functions with increasing strain and temperature, down to the level of noise-like fluctuations. This level is, in turn, influenced by the count in Rayleigh scattering spectra. Its increase leads to a reduction in fluctuation level. On the other hand, the smaller the count, the better the speed performance. The count in spectra is determined by the TF tuning step. The step was chosen to be 0.05 nm, which is about one-third of the filter bandwidth (0.17 nm) and allows one to obtain contrast cross-correlation functions at an acceptable total number of steps: 121. At a tuning step approximately equal to or exceeding the TF bandwidth, we would obtain weakly correlated or uncorrelated Rayleigh scattering spectra and, hence, it would be impossible to evaluate the shift of the spectra. Thus, we conclude that, at a known TF bandwidth, there is a quasi-optimal tuning step which ensures both high contrast of cross-correlation functions and an acceptable speed of the sensor.

WDM3 is used as both a directional spectral filter and a means of organising a reflectometric channel for Raman scattering. The transmission range of the shorter wavelength port of WDM3 is 1450–1490 nm, and that of its longer wavelength port is 1530–1580 nm. In addition, the Raman scattering channel includes PD2, similar in characteristics to PD1.

PD1 and PD2 are interfaced to a computer via eight-bit analog-to-digital converters (ADC1 and ADC2, respectively) operating at a sampling rate of 10^8 Hz. The computer controls the TF and ensures data acquisition and storage. After spectral scanning, the data are used to evaluate the measured parameters.

In addition to the above devices, the scheme includes an approximately 8-km length of Corning SMF-28e single-mode sensing fibre (SF). Its end portion has a temperature-controlled segment (S1) about 35 m in length (enclosed in a thermal chamber) and a strain-controlled segment (S2) 9 m in length [secured in the supports of a tension control system (TCS)]. The TCS includes a system of two supports, one fixed on a common base and the other fixed on the nut of a 'screw–nut' mechanism. The separation between the supports is controlled by rotating its handle. Each support has one flat metallic plate hinged to it, with a straight fibre segment cemented to the plate. Thus, all measures are taken to avoid bending losses.

3. Experimental

In our experiments, the strain and temperature were measured in the following sequence:

(1) measuring reference Rayleigh scattering spectra and a reference anti-Stokes Raman signal under initial conditions (25 °C and zero tension);

(2) heating S1 to 45 °C and stretching S2 to 200 με at constant temperature;

(3) measuring the Rayleigh scattering spectra and anti-Stokes Raman signal;

(4) calculating the difference signals $\Delta\Lambda$ and $\Delta P_{\mathrm{RAS}}^{\mathrm{N}}$ and determining the sensitivity coefficients that appear in the matrix equation (2) (the external influences in segments S1 and S2 were measured by an independent technique); and

(5) solving Eqn (2) for the changes in strain $\Delta\varepsilon$ and temperature ΔT.

The measurements of both the reference and test spectra took 10 min.

Figure 4 shows graphs of the $\Delta\Lambda$ and $\Delta P_{\mathrm{RAS}}^{\mathrm{N}}$ signals obtained. Since segments S1 and S2 were independently exposed to temperature and strain, respectively, determining the sensitivity coefficients in the matrix equation (2) reduces to calculating the ratios of the average levels of the $\Delta\Lambda$ and $\Delta P_{\mathrm{RAS}}^{\mathrm{N}}$ signals in these segments to the corresponding changes in temperature (20 °C) and tension (200 με). As a result, the following values were obtained:

$$S_{\varepsilon}^{\Lambda} = 1.2 \text{ pm } \mu\varepsilon^{-1}; \quad S_{T}^{\Lambda} = 11 \text{ pm } ^{\circ}\mathrm{C}^{-1}; \qquad (3)$$

$$S_{T}^{\mathrm{RAS}} = 7.2\times10^{-3} \ ^{\circ}\mathrm{C}^{-1}.$$

These values are similar to those reported previously [8–10].

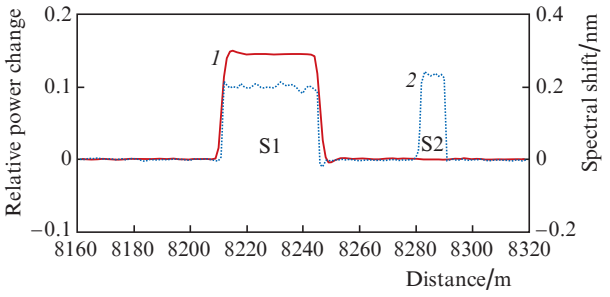

Figure 4. (*1*) Relative change in the anti-Stokes power, $\Delta P_{\mathrm{RAS}}^{\mathrm{N}}$, and (*2*) shift of the Rayleigh scattering spectrum, $\Delta\Lambda$, as functions of the distance from the fibre input.

It is seen from Fig. 4 that the change in anti-Stokes power $\Delta P_{\mathrm{RAS}}^{\mathrm{N}}$ (curve *1*, segment S2) has a low sensitivity to strain, so $S_{\varepsilon}^{\mathrm{RAS}}$ cannot be evaluated with satisfactory accuracy in the framework of this study. It is reasonable to use the following value obtained previously [10]:

$$S_{\varepsilon}^{\mathrm{RAS}} = -1.6\times10^{-6}\ \mu\varepsilon^{-1}. \quad (4)$$

Figure 5 shows $\Delta\varepsilon$ and ΔT evaluated by solving Eqn (2) with allowance for (3) and (4). The rms noise levels evaluated in the range 7600–8200 m are 1.1 με and 0.04 °C for the strain and temperature changes, respectively.

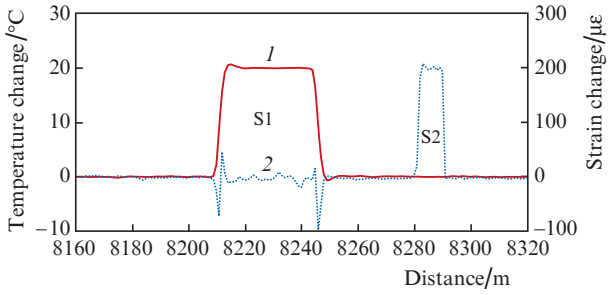

Figure 5. Results of simultaneous (*1*) temperature change ΔT and (*2*) strain change $\Delta\varepsilon$ measurements (derived from the data in Fig. 4).

The artefacts in the form of prominent spikes in the calculated strain change on the boundaries of S1 (Fig. 5), where mechanical strain is negligible, originate from the fact that the edges of the $\Delta\Lambda$ and $\Delta P_{\mathrm{RAS}}^{\mathrm{N}}$ signals differ in slope (Fig. 4). The distinction between the edge slopes is due to the dispersion in the fibre and the fundamentally different signal processing procedures in the Rayleigh and Raman channels. It seems likely that the temperature and mechanical stimuli occurring in practice will have less sharp spatial edges in comparison with our experiments, which will allow one to avoid such artefacts. It cannot be ruled out that artefacts can be minimised by improving data processing algorithms.

In addition to the artefacts, there are parasitic noise-like fluctuations $\Delta\varepsilon$ in segment S1. Their standard deviation is 6 με (evaluated in the artefact-free range from 8213 to 8244 m), which considerably exceeds the calculated deviation of 1.1 με in the range 7600–8200 m, where the fibre was not subject to external influences. The fluctuations were found to increase linearly with increasing temperature changes relative to a reference. Under the assumption that the standard deviation of the fluctuations is a linear function of temperature change, it is easy to estimate their temperature sensitivity coefficient, which is approximately 0.24 με °C^{-1}. This value can be thought of as an additional temperature-related uncertainty. According to our observations, uncertainties always increase as the external influences to be evaluated become farther away from reference conditions. We attribute this to specific features of correlation processing.

4. Conclusions

We have experimentally demonstrated the possibility of separately sensing temperature changes and longitudinal strain in an optical fibre using a hybrid distributed sensor based on measurements of the anti-Stokes Raman signal and Rayleigh scattering spectra via probe light frequency tuning with a computer-controlled microelectromechanical filter. The present results lead us to conclude that the proposed scheme is potentially attractive for practical application in infrastructure health monitoring.

References

1. Parker T.R., Farhadiroushan M., Handerek V.A., Rogers A.J. *IEEE Photonics Technol. Lett*., **9**, 979 (1997).
2. Alahbabi M.N., Cho Y.T., Newson T.P. *Opt. Lett*., **29**, 26 (2004).
3. Liu X., Bao X. *J. Lightwave Technol*., **30**, 1053 (2012).
4. Alahbabi M.N., Cho Y.T., Newson T.P. *Opt. Lett*., **30**, 1276 (2005).
5. Bolognini G., Soto M.A., Pasquale F.D. *IEEE Photonics Technol. Lett*., **21**, 1523 (2009).
6. Kishida K., Yamauchi Y., Guzik A. *Photonic Sens.*, **4**, 1 (2014).
7. Froggatt M., Moore J. *Appl. Opt*., **37**, 1735 (1998).
8. Koyamada Y., Imahama M., Kubota K., Hogari K. *J. Lightwave Technol*., **27**, 1142 (2009).
9. Gorshkov B.G., Taranov M.A., Alekseev A.E. *Laser Phys*., **27**, 085105 (2017).
10. Gorshkov B.G., Gorshkov G.B., Taranov M.A. *Laser Phys. Lett*., **14**, 015103 (2016).